Differential thermography for experimental, full-field stress analysis of hip arthroplasty

ELECTRONIC VERSION OF AN ARTICLE PUBLISHED AS [J MECH MED BIOL 10,2,2010,515-529] [DOI:10.1142/S0219519410003496]

DIFFERENTIAL THERMOGRAPHY FOR EXPERIMENTAL, FULL-FIELD STRESS ANALYSIS OF HIP ARTHROPLASTY

ELISABETTA M. ZANETTI

DIIM, University of Catania, Vle Andrea Doria 6
Catania, 95125, ITALY
elisabetta.zanetti@diim.unict.it

ALBERTO L. AUDENINO

DIMEC, Politecnico di Torino, Cso Duca degli Abruzzi 24
Torino,10129, ITALY
alberto.audenino@polito.it

A hip prosthesis implant produces a significant deviation in the stress pattern compared with the physiologic condition. Stress patterns are here evaluated experimentally on synthetic femurs, by means of thermoelastic stress analysis.
Two factors have been considered: stem implantation and head offset. Stress maps were obtained using differential thermography and correlated to these factors.
Thermoelastic stress maps have demonstrated to be sensitive to the implant and the head offset. In detail, the standard deviation of stresses can reduce from –5% to –50% (with reference to the physiologic one), depending on stem design; peak stresses change their position or disappear for different implant position or press-fitting, the sensitivity of average stresses to the offset is at least equal to 0.07 MPa/mm.
On the whole, a methodology was developed, allowing the experimental evaluation and comparison of the stress distributions produced by different implants.

Keywords: Thermoelastic stress analysis, hip implant, synthetic femur

1. Introduction

It is well known that a hip prosthesis implant produces a deviation in the stress pattern compared with the physiologic condition;[1,2] according to Wolff's law,[3] bone adaptation effort can be related to the amount of this deviation, so it can give a sound criterion for the comparison of different configurations of bone-implant systems[4] in the stage of surgical pre-planning, and for understanding the in vivo response of existing as well as new designs in the phase of pre-clinical testing,[5] where the combination of experimental and numerical methods has proven to be synergetic.[6,7]
The experimental analysis of stress patterns can be accomplished through both localized measurements and full-field techniques.[8,9]
The former can give very precise information: all stress components can be determined. However the most critical areas must be identified a priori and a large number of measurements must be performed in order to have an idea of stress flow from the femoral head to the femoral diaphysis. Full-field techniques are more suited to providing a

global representation of stress pattern, while their main limitations are: mapping just one scalar variable that is a combination of the principal stresses and, in most cases, the need to prepare specimens.
Photoelasticity is one of the most commonly applied full-field techniques in orthopedic biomechanics.[10,11,12] In this case, specimen preparation is quite complex: the femur needs to be coated with a birefringent material of uniform thickness (or at least of known thickness at every point). Furthermore, the analysis of results is not immediate and numerical data can be obtained only at fixed locations.
More recently, another full-field technique has been developed: Thermoelastic Stress Analysis (TSA);[13] TSA employs special infrared detectors and signal processing equipment to image temperature changes that correspond to the first stress invariant, produced by dynamic loads in a structure.[14] Duncan[15] introduced an extensive critical analysis of the advantages and disadvantages of TSA, and subsequently performed a similar study that analyzed a fresh human femur and calibrated the results against strain gauge readings.
The goal of the present study was to develop and test a methodology for performing quantitative thermoelastic stress analysis on synthetic femurs. As a benchmark, the stress distributions produced by two stem models, each implanted twice, realizing five different head offsets, were used.

2. Materials and Methods

2.1 Specimens

Tests were conducted on five composite femurs (mod. 3306, Pacific Research Labs, Vashon Island, WA), which are similar in shape, mechanical characteristics, and material density to those of human femurs. [8,16] Synthetic femurs were chosen to reduce interspecimen variability.
Femur 1 was not implanted, while two different stem designs were press fitted into broached canals of femora 2-3 (stem A) and of femora 4-5 (stem B), by orthopedic surgeons, following the respective protocol; implanted femurs were inspected with CT scans in order to verify stem positioning (Figure 1). Both stems are tapered and are still being implanted after ten years with excellent clinical results; stem A has a circular cross-section and is made of titanium, while stem B has a rectangular cross-section and is made of a titanium alloy. Table 1 reports head offset for the five specimens coupled to four different heads.
All femora were sprayed with a special paint with constant high emissivity.

Table 1. Head offset produced by different head sizes (underlined values refer to tested configurations)

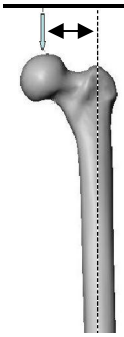

	Head size**			
Implant I(N)*	S=-5	M=0	L=+4	XL=+12
A(2)	40.95	44.73	<u>47.75</u>	53.78
A(3)	<u>42.17</u>	45.94	<u>48.96</u>	<u>55.00</u>
B(4)	44.37	<u>48.14</u>	51.16	57.20
B(5)	<u>43.39</u>	47.11	<u>50.08</u>	<u>56.03</u>
Physiologic(1)		<u>49.41</u>		

*I is identifies the prosthesis model; N identifies the femur
** Head size is related to the depth of the coupling cone between the femoral head and neck

2.2 Program of trials

Table 2 reports the program of trials for thermoelastic stress analyses.

Table 2. Program of trials

Trial	Compared stress maps (Stem implant - Head)				
1	Intact	A(2)-L	A(3)-L	B(5)-L	B(4)-M
2	Intact	A(3)-S	A(3)-L	A(3)-XL	
3	Intact	B(5)-S	B(5)-L	B(5)-XL	

The stress distribution is mainly influenced by two factors: the implant that is the stem model and its position inside the femoral cavity (factor I), and the moment arm of the articular force (factor II). Factor I was evaluated in

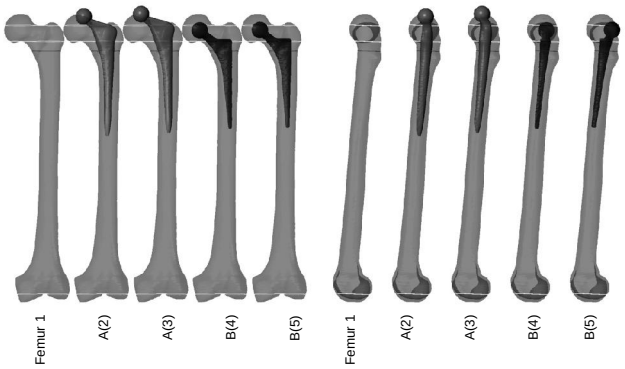

Fig. 1. Anterior (left) and medial (right) views of the femurs

Trial #1: given a specific implant, the head that produced the moment arm closest to the physiologic condition was tested (see Table 1, bold typed characters). Factor II was examined in Trial #2 (stem A) and in Trial #3 (stem B). The small sample size (four implanted specimens for factor I, and three head offset with replication for factor II) did not allow the authors to numerically quantify one further factor that is stem model (its effect is here mixed with implant position); the quantitative evaluation of this aspect would require a very large number of specimens and considering various femurs, as discussed in the last section.

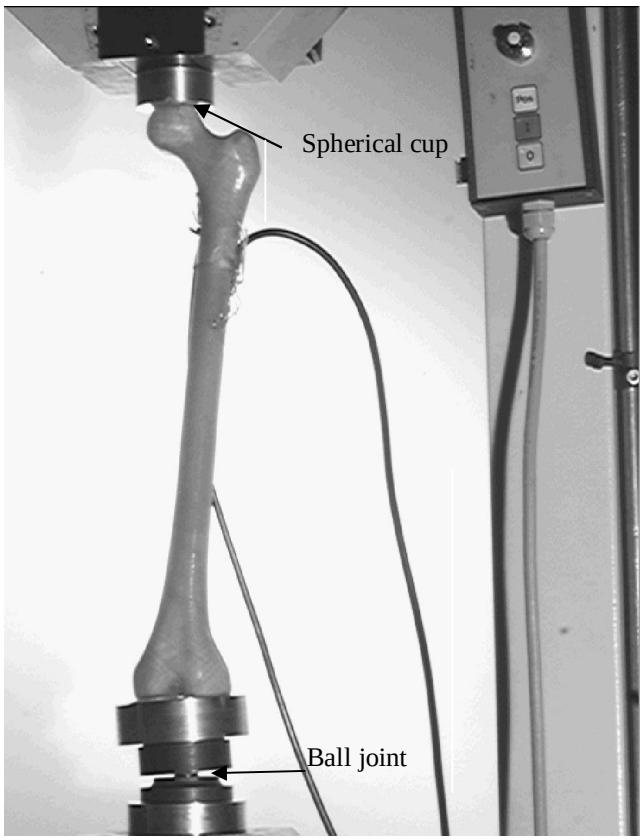

Fig. 2. Loading rig

2.3 Loading rig

The loading rig used (Figure 2) was specifically developed for experimental tests on femora: its main features are that it is not over-constrained (the femur lies between two spherical hinges),[8] and both static and dynamic loads can be applied with frequencies up to 10 Hz, as required by TSA.

The dynamic vertical load (925.0±578.5 N, 10 Hz) was applied using an Instron testing machine (mod. 8872, Milan, Italy), the frequency proved to be sufficiently high in order to achieve adiabatic conditions, and the load amplitude was chosen to simulate a physiologic load under static conditions (2 BW peak-to-peak load). A reduced body weight has been considered (578.5 N) because higher values (we reached 1503.5 N peak load) would cause excessive displacements, making it difficult to perform a correct TSA. Most authors consider also abduction loads[17] and eventually torsional loads;[1,18] the physiologic loading condition has been simplified here in order to allow the application of dynamic loads.

2.4 Thermographic image acquisition

Full field thermoelastic maps were acquired using a differential thermocamera, (Deltatherm1500, Stress Photonics, Madison, WI); the camera resolution was 320x256 pixels (spatial resolution was equal to 1.1 pixel/mm for frames where the proximal half of the femur was imaged, and reached 2.7 pixels/mm in detailed frames where, only the proximal area was acquired, being the most critical, Figure 3), and image sampling frequency was equal to 105 Hz; thermographic images were acquired from four perspectives (anterior, posterior, medial and lateral). Each implant was loaded 10 times (reassembling the load setup between the repetitions), and a good repeatability was measured (0.94 MPa maximum standard deviation).

2.5 Anisotropic material and calibration

According to thermoelastic theory,[14] temperature maps can be converted into the maps of the first stress invariant once the calibration constant has been calculated, adiabatic conditions have been reached, and plane-isotropy has been demonstrated (in the case of ortothropy, further assumptions need to be made[19,20,21]):

$$\Delta T = -K_m T \cdot \Delta I_{1,\sigma}, \qquad (1)$$

where:

- K_m is the thermoelastic constant of the material (measured through calibration);
- T is the absolute ambient temperature;
- $\Delta I_{1,\sigma}$ is the first stress invariant;
- ΔT is the amplitude of temperature variation, measured by the differential thermocamera.

A full characterization would have required specimens cut from the same sheet, at several orientations but the authors considered that, for this material (short glass fiber reinforced epoxy resin), tests performed on two orthogonal directions may confirm the hypothesis of plane-isotropy; the two series of specimens were sized 30x2x60 mm and were loaded at 8.00±7.00 MPa. The results showed very similar calibration factors (their difference was lower than 0.7%), confirming material isotropy and allowing the quantitative application of TSA.

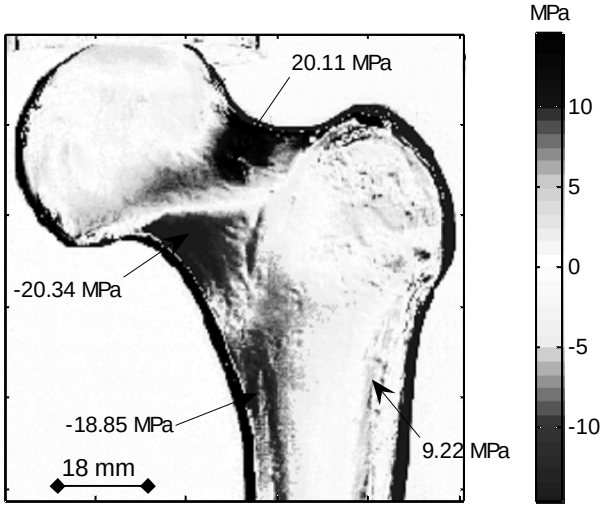

Fig. 3: Detailed map of the first stress invariant

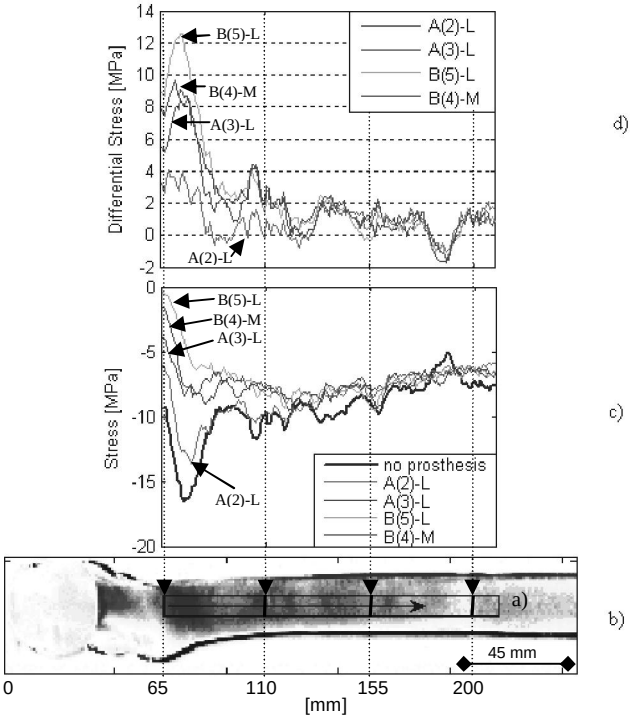

Fig. 4 Trial #1, medial view - Axial Stress analysis - a) AOI; b) reference axis; c) mean stresses (column by column) vs. axial position; d) differential stresses with reference to the unimplanted femur

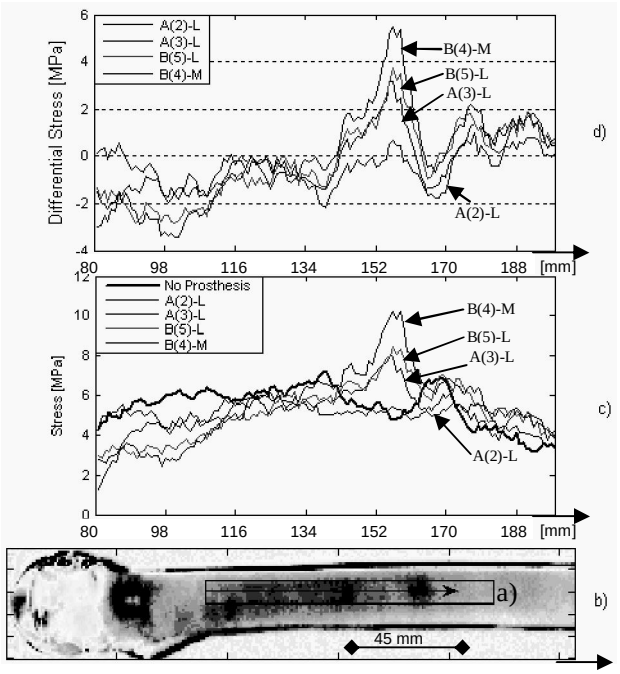

Fig. 5 Trial #1, lateral view - Axial Stress analysis - a) AOI; b) reference axis; c) mean stresses vs. axial position; d) differential stresses vs axial position

2.6 Analysis of thermoelastic maps

Thermoelastic maps were exported to Matlab™ and were compared in three different ways. Visual comparison was the most immediate analysis; a second methodology relied on the analysis and comparison (through Kolmogorov-Smirnov test) of the statistical distributions of stress: homologous Areas Of Interest (AOI) were selected on the femurs, and stress probability density, the maximum, minimum and average stress level and the standard deviation of stress were computed (a lower standard deviation means a more uniform distribution). The third comparison considered the stress pattern along the diaphyseal axis.

3. Results

The experimental methodology introduced here was tested comparing different bone-implant systems; as detailed in the previous section, two factors were considered.

3.1 Factor I

The same stem implanted in the same femur, can produce different stress distributions, due to variations in the implant position and press-fitting (Figure 1). In particular, the medial view (Figure 4) shows different axial stress patterns in the proximal area of A(2)-L and A(3)-L. The peak stress located under the neck in the unimplanted femur and in A(2)-L is absent in A(3)-L (mean stress differences between A(2)-L and A(3)-L range from 2 to 4 MPa). On the contrary, in the lateral view (Figure 5) the peak stress located in the mid diaphysis of A(3)-L is absent in A(2)-L.

Table 3: Statistical data concerning trial #1- Posterior and Lateral Views

	Min [MPa]	Max [MPa]	Mean [MPa]	St. deviation [MPa]*
		Posterior view		
(1)	-10.29	8.21	-1.62	3.21
A(2)-L	-12.22	15.39	-1.33	3.07 (-4%)
A(3)-L	-12.42	16.42	-0.58	3.02 (-6%)
B(5)-L	-4.80	13.90	-0.41	1.58 (-51%)
B(4)-M	-5.92	5.84	-0.98	1.66 (-48%)
		Lateral View		
(1)		8.23	4.18	1.76
A(2)-L		7.54	4.18	1.36 (-23%)
A(3)-L		9.51	4.55	1.33 (-24%)
B(5)-L		11.35	4.45	1.85 (+5%)
B(4)-M		11.42	4.24	2.18 (+24%)

*The percentage standard deviation refers to the unimplanted femur

In the posterior view (Table 3 and Figure 6), A(2)-L and A(3)-L show similar stress distribution shapes and standard deviations, but present a slight difference in the means: one stress distribution is slightly shifted with respect to the other. It is therefore plausible that the stem was located differently in A(2)-L and A(3)-L, with a slight extra rotation in the frontal plane in the case of the second implant; this evaluation was confirmed by the measurement of specimens in CT scans: A(2)-L showed 11° anteversion, A(3)-L showed 13° anteversion.
The combined influence of stem model and repeated implant could be assessed from trial #1 as well. In the posterior view, the proximal area (Figure 6, top image) shows an under-loading due to stress shielding, which is more pronounced in stem B. This behavior is also confirmed by the stress probability density function (Figure 6, graph) and statistical parameters (Table 3): both B(4) and B(5) show a more uniform stress distribution (standard deviation is about -50% vs. -5% of models A) and smaller peak compressive and tensile stresses. The statistical comparison of stress distributions through KS test, testifies that all distributions are significantly different from one another ($p<0.001$).
Looking at the stress distributions along the diaphysis, the medial view (Figure 4a) always shows the highest stress concentration in the proximal region, with a peak just below the stem neck.
However, in every implanted specimen, there is clear under-loading of this area compared to the unimplanted condition (Figure 4d). The greatest differences in stress are found with stems B (in this area, differential stress ranges from 7.70 to 12.58 MPa vs. 5.19 to 8.49 MPa of A(3)-L and 2.83 to 4.09 MPa of A(2)-L). Moving to more distal areas, the stresses become very close to the unimplanted condition with no significant differences between the two stem models. The lateral view (Figure 5a) shows that the most stressed area of the unimplanted femur, localized in the subtrochanteric region, is totally absent in the implanted femora.

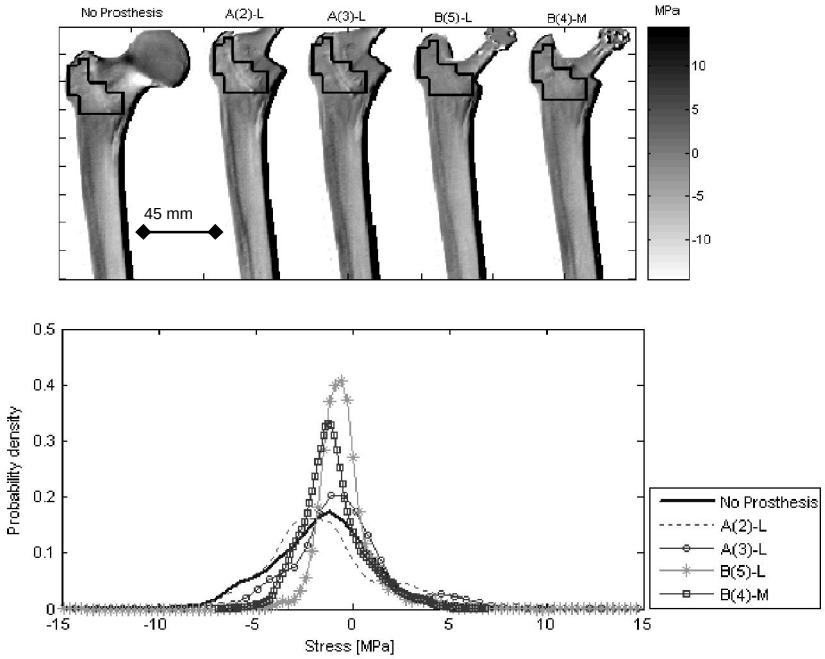

Fig. 6 Trial #1, posterior view; top image: maps of the first stress invariant and outline of the Area Of Interest (AOI); bottom image: statistical distribution of stresses.

In particular, B stems appear to be unstressed in this area. More distally, the axial stress patterns (Figures 5c, d) show, for the implanted femora, an under-loading (differential stress ranging from -3.51 to -2.79 MPa) along the proximal diaphysis together with heavily stressed and concentrated areas in the mid diaphysis. Also in this case, wider stressed areas and greater stress differences (differential stress ranging from 3.72 to 5.48 MPa) are present in B stems (Figure 5d). An interesting observation was that two different patterns characterized the anterior and posterior view. Thus it is useful to consider both views, which may also allow the identification of an incorrect neck anteversion: anteversion produces a flexural oment around the medial-lateral axis.

3.2 Factor II

The influence of the head offset can best be appreciated in the stress maps obtained in the lateral (Figure 7, left images) and medial views (Figure 7, right images), regarding trials #2 (A stem, top images of Figure 7) and #3 (stem B, bottom images of Figure 7). The peak stresses are plotted against the offset in Figure 8. In the lateral view, both models show important overloading compared to the unimplanted femur: peak stress increases as the offset increases, and stem A is found to be more sensitive (higher gradient of line) than stem B. In the medial view, peak stresses were always lower than the in the unimplanted femur, even at the highest offset values. This is due to an important under-loading of the neck region. In this view, stem B is found to be more sensitive to the offset.
Overall, it was demonstrated that the head offset always has considerable influence on the peak stress values.

4. Discussion and Conclusions

Thermoelasticity is an appealing technique because specimen preparation is simple since it is only necessary to paint the femur black, while the measurements do not require any contact with the specimen and can be performed in complex geometric structures. Furthermore, data analysis is immediate because the technique provides full-field stress maps of the first stress invariant (which is also the principal stress in the case of an uniaxial stress field, as in the femur diaphysis subjected to flexural moments). The main drawbacks are the high cost of instrumentation, its critical use with anisotropic materials,[20] the need to work on surfaces with high emissivity, and the need to dynamically load the specimens.

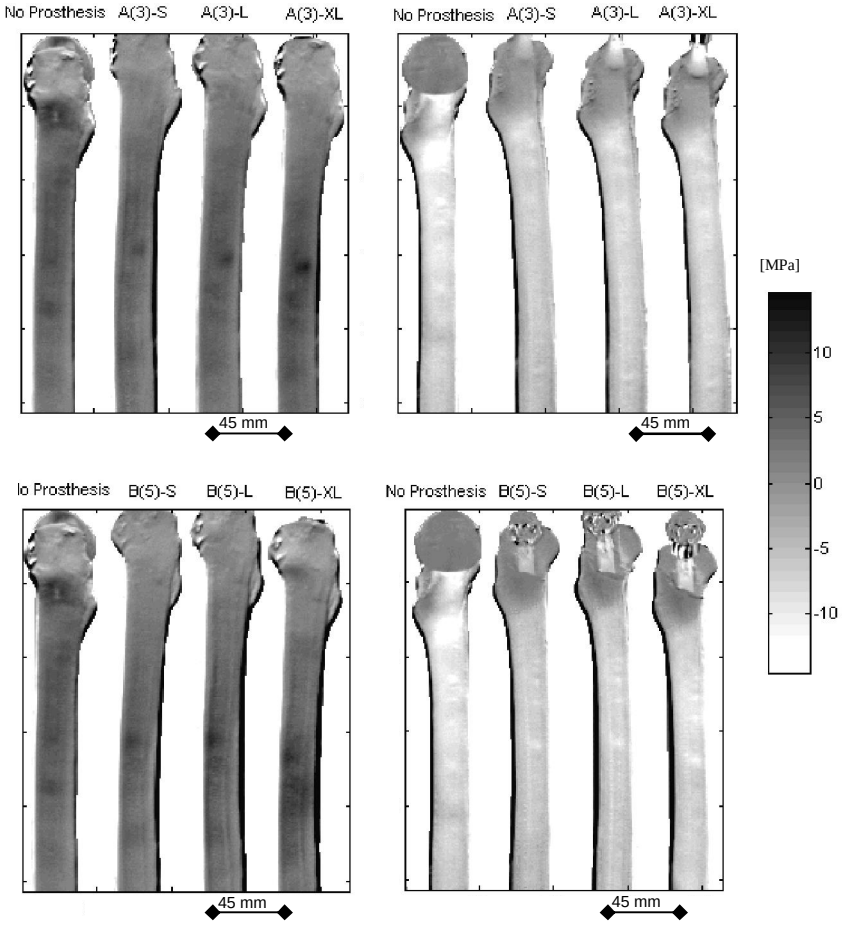

Fig- 7 Trials #2 (top) and #3 (bottom)– Lateral (left) and Medial (right) views: maps of the first stress invariant

In biomechanics, thermoelastic stress analysis was seldom used, mostly in a qualitative manner; a preliminary study was performed on uniaxially loaded cortical bone cubes[22]; in a more recent study, the same authors applied thermography to canine femora,[23] calibrating the results on the basis of strain gauge readings; however it is not specified how they manage bone anisotropy: differential thermography cannot be applied in generic anisotropic materials.[19]

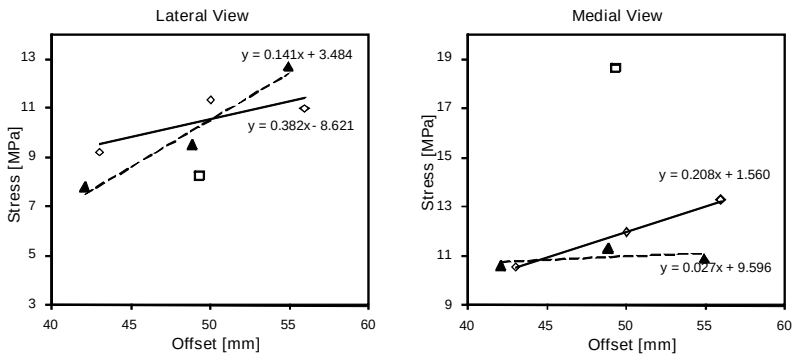

Figure 8: Offset influence: peak stresses vs. head offset in lateral (left graph) and medial (right graph) views; □ unimplanted femur, ▲ stem A, ◊ stem B

Kruger-Franke et al.[24] describe another investigation that considered dried human femurs. Here, the TSA results were compared with strain gauge measurements to demonstrate their quantitative value. Refior et al.[12] employed fresh specimens and tested implanted femurs. In this case, the surfaces could not be coated with black paint, a

major shortcoming in the experimental procedure, since emissivity is low and cannot be regarded as constant over the entire specimen. Results were assessed from a qualitative standpoint and were compared with photoelastic maps, showing good agreement. However, no details are given regarding how the authors allowed for the fact that photoelastic maps reproduce the pattern of the difference of the main strains, while thermoelastic maps reproduce the pattern of the first strain invariant (i.e., the sum of main strains).

One of the limits of the present study is that loading condition has been simplified and only the situation immediately following implantation can be simulated: there is neither biological fixation or bone remodeling. In Duncan,[15] the complexity of the experimental set up limited maximum loading frequency to 6 Hz, which might interfere with achieving the adiabatic condition required by TSA. In the opinion of the authors, the simplifications of loading condition can be tolerated because the final aim of the study is not femur strength assessment, but the comparison of femoral stress patterns in different configurations. The authors demonstrate that an overview of different performances produced by various implants can be reached and is particularly evident here because it is a full-field analysis and the number of measurement points is not limited as for strain gauge analysis; besides, more complex loading could be analyzed through numerical models: this experimental set-up allows direct, full-field validation of a FE model.[25] The validated numerical model can allow the quantification of stem-bone related phenomena (considering different bone geometries, slight variations of implant position, etc.), leading to patient-specific reasoning; it can also indicate critical areas to be noted during experimentation, and can provide further information: the full stress tensor, internal bone stress analysis and interface analysis.

The decision to use synthetic femurs was due to difficulties in finding, handling and preserving real bones. Moreover, synthetic bones have physical properties similar to real bones and provide lower variability in testing.[16]

The general stress distribution on intact femora is similar to the one described by other authors who used strain gauges[17] or photoelastic coating;[12] generally speaking, the femur is subjected to a flexural moment, so its medial side undergoes compressive stresses, while its lateral side undergoes tensile stresses.

It should be emphasized here that TSA allows the evaluation of the only dynamic component of loads; the effect of press-fitting cannot be appreciated: it would require the acquisition of the press-fitting phase as well, and complex image analyses of its transitory signal.

The experimental evaluation of stress pattern deviations from the physiologic condition in synthetic implanted femurs, produced results in accordance with well known considerations.

The stress distributions proved to be influenced by the implant geometry: even the same stem implanted more than once may produce different results; in particular, neck version plays an important role; other authors emphasized the importance of this aspect in strain distribution along the diaphysis.[26]

The study demonstrated how the comparison between different stem models is here particularly evident because it is a full-field analysis and the number of measurement points is not limited as is for strain gauge analysis; stem B appeared to produce a better performance. As a matter of fact, experimental thermography can here allow only a qualitative assessment of different stems performance: the respective numerical quantification would require a higher number of implants of the same stem, and the employment of an apposite rig in order to make implant position more repeatable; in the opinion of the authors, a numerical analysis through a validated numerical model is more suitable to this task. In fact, it would be too onerous (both in terms of time and cost) to experimentally replicate the variability of stem positioning and press-fitting; in literature, most studies of this kind consider just three repeated implants, however, analyzing such a limited number of specimens would bear strong implications, in relation to the present inquiry: a quite rough estimate of result variability might be obtained, considering that the 95% confidence interval for the population standard deviation ranges from 0.5 to 6.2 experimental std (according to the chi square distribution); parametric tests for comparing means (like T test) cannot be properly applied unless the original population is proven to be normally distributed; finally, the experimental results would still be incomplete, being confined to the analysis of the synthetic femur, so only the performance of the stem in relation to this specific geometry and mechanical properties would be estimated.

The influence of head offset was also assessed: in all cases, a higher offset produces higher stresses; but sensitivity to this parameter changes depending on the stem model. This aspect has been broadly documented in literature.[18,27]

The limited number of cycles required to perform each test (some hundred cycles) is not likely to produce any fatigue sign in the material.

Acknowledgements

This research was funded by the Italian Ministry of University and Research, Program name: PRIN 2004.

Many thanks to Prof. Galietti who has borrowed us the differential thermocamera and who took part to the arrangement of experiments, to Giovanna Consoli and Stefano Musso for their active contribution to both numerical and experimental work.

References

1. Aamodt A, Lund-Larsen J, Eine J, Andersen E, Benum P, Husby OS, Changes in Proximal Femoral Strain After Insertion of Uncemented Standard and Customised Femoral Stems. An Experimental Study in Human Femora, J Bone Joint Surg [Br] 83: 921-929, 2001.
2. Bobyn JD, Mortimer ES, Glassman AH, Engh CA, Miller JE, Brooks CE, Producing and Avoiding Stress Shielding. Laboratory and Clinical Observations of Noncemented Total Hip Arthroplasty, Clin Orthop Relat Res 274: 79-96, 1992.
3. Wolff J, Das Gesetz der Transformation der Knochen, Verlag von August Hirschwald, Berlin, 1982.
4. Huiskes R, Stress patterns, failure modes, and bone remodeling, in Fitzgerald R Jr (ed.), Non-cemented hip arthroplasty, Raven Press, New York, pp. 283-302, 1988.
5. Prendergast PJ, Maher SA, Issues in pre-clinical testing of implants, J Mater Process Technol, 118: 337-342, 2001.
6. McNamara BP, Cristofolini L, Toni A, Taylor D, Relationship between Bone-Prosthesis Bonding and Load Transfer in Total Hip reconstruction, J Biomech 30: 621-630, 1997.
7. Viceconti M., Cristofolini L., Baleani M., Toni A, Pre-clinical validation of a new partially cemented femoral prosthesis by synergetic use of numerical and experimental methods, J Biomech 34: 723-731, 2001.
8. Zanetti EM, Bignardi C, Chapter VI: Structural Analysis of Skeletal Body Elements: Numerical and Experimental Methods, in Leondes CT (Ed), Biomechanical Systems Technology, Vol. 3: Muscular Skeletal Systems, World Scientific Publishing Company, London, pp. 185-225, 2009.
9. Harwood N, Cummings WM, Thermoelastic Stress analysis, Adam Hilger, New York, 1991.
10. Milch H, Photo-elastic Studies of Bone Forms, J Bone Joint Surg 22: 621-626, 1940.
11. Pawels F, Biomechanics of the normal and diseased hip: theoretical foundation, technique and results of treatment, Springer-Verlag, Berlin, 1976.
12. Refior HJ, Schidlo C, Plitz W, Heining S, Photoelastic and Thermoelastic Measurements of Stress on the Proximal Femur Before and After Implantation of a Hip Prosthesis With Retention of the Femoral Neck, Orthopedics 25: 505-511, 2002.
13. Rauch BJ, Rowlands RE, Thermoelastic Stress Analysis, in Kohayashi AS (ed.), Handbook of Experimental Mechanics, VCH Publishers, New York, pp. 581-599, 1993.
14. Thomson W, On the Dynamical Theory of Heat, Trans Roy Soc Edimbourg 20: 261-83, 1853.
15. Duncan JL, Strain Measurement by Thermoelastic Emission, in Miles AW, Tanner KE (eds.), Strain measurement in biomechanics, Chapman&Hall, London, pp. 157-168, 1992.
16. Cristofolini L, Viceconti M, Cappello A, Toni A, Mechanical Validation of Whole Bone Composite Femur Models, J Biomech 29: 525-35, 1996.
17. Gillies RM, Morberg PH, Bruce WJM, Turnbull A, Walsh WR, The Influence of Design Parameters on Cortical Strain Distribution of a Cementless Titanium Femoral Stem, Med Eng Phys 24: 109-114, 2002.
18. Otani T, Whiteside LA, White SE, The Effect of Axial and Torsional Loading on Strain Distribution in the Proximal Femur as Related to Cementless Total Hip Arthroplasty, Clin Orthop Relat Res 292: 376-383, 1993.
19. Audenino AL, Calderale PM, Assessment of Thermoelastic Strain Analysis on composite femur model, IFMBE Proceedings (CD) 452, pp.1-4, 2004.
20. El-Hajjar R, Haj-Ali R, IR-thermography for strain analysis in pultruded fiber reinforced plastics, Experimental Techniques 28:19-22, 2004.
21. Ju SH, Rowland RE, Thermoelastic Determination of KI and KII in an Orthotropic Graphite-Epoxy Composite, Journal of composite materials, 37: 2011-2025, 2003.
22. Vanderby R Jr, Kohles SS, Thermographic Stress Analysis in Cortical Bone, J Biomech Eng 113: 418-22, 1991.
23. Kohles SS, Vanderby R Jr, Thermographic Strain Analysis of the Proximal Canine Femur, Med Eng Phys. 19: 262-266, 1997.
24. Kruger-Franke M, Heiland A, Plitz W, Refior HJ, Thermo-Elastic Stress Analysis of Human Bones, Z Orthop Ihre Grenzgeb, 133: 389-393, 1995.
25. Stolk J, Verdonschot N, Cristofoloni L, Toni A, Huiskes R, Finite element and experimental models of cemented hip joint reconstructions can produce similar bone and cement strains in pre-clinical tests, J Biomech, 35: 499-510, 2002.
26. Umeda N, Saito M, Sugano N, Ohzono K, Nishii T, Sakai T, Yoshikawa H, Ikeda D, Murakami A, Correlation Between Femoral Neck Version and Strain on the Femur After Insertion of Femoral Prosthesis, J Orthop Sci, 8: 381-386, 2003.
27. Charles MN, Bourne RB, Davey JR, Greenwald AS, Morrey BF, Rorabeck CH, Soft-Tissue Balancing of the Hip, the Role of Femoral Offset Restoration, Instr Course Lect 54: 131-141, 2005.